Sequential State Estimation for Electrophysiology Models with Front Level-Set Data Using Topological Gradient Derivations

Annabelle Collin, Dominique Chapelle, Philippe Moireau

Sequential state estimation for electrophysiology models with front level-set data using topological gradient derivations

A. Collin*, D. Chapelle and P. Moireau

Inria Saclay Ile-de-France, *MΞDISIM* Team, Palaiseau, France

Abstract. We propose a new sequential estimation method for making an electrophysiology model patient-specific, with data in the form of level sets of the electrical potential. Our method incorporates a novel correction term based on topological gradients, in order to track solutions of complex patterns. Our assessments demonstrate the effectiveness of this approach, including in a realistic case of atrial fibrillation.

Keywords: electrophysiology modeling; data assimilation; estimation; observer; bidomain equations; topological gradient; shape derivative

1 Introduction

Our objective in this paper is to propose an effective strategy for performing estimation in an electrophysiology model with data in the form of level sets of the electrical potential, as e.g. with isochrones of the depolarization front reconstructed in electrocardiographic imaging [15, 9]. Estimation is a crucial step for obtaining a personalized model – typically for a patient – that can be used for predictive purposes, with a view to providing diagnosis and prognosis assistance in the clinics [17].

Previous works have already considered the issue of state and/or parameter estimation in electrophysiology models, see e.g. [14, 12, 9] and references therein. Here, we depart from most existing works by proposing an estimation method of so-called *sequential* type, namely, consisting in a dynamical system obtained by incorporating in the original model a correction taking into account the discrepancy between the current simulation and the data. Sequential estimation – or data assimilation – methods have already been shown to be extremely effective for a variety of models and data, including in cardiac modeling applications with real data [2], albeit must be adapted to each category of model and data of concern. In our case, we will consider a bidomain model [5], without resorting to any model reduction or transformation – e.g. into eikonal-curvature equations – and address the issue of devising a sequential estimation method well-suited to the above type of data, including in cases where multiple fronts with little structure are present in the solution, as typically in fibrillation scenarii.

* Current affiliation: Università di Pavia, Italy

In the next sections we present in sequence the problem setting (Section 2), the proposed estimation methodology (Section 3), and detailed assessment results including a realistic complex fibrillation case (Section 4), before providing some conclusions.

2 Problem setting

2.1 Model

We consider the surface bidomain model proposed in [4], particularly well-suited to the atria very thin walls [7]. This model is posed on the midsurface of the wall $\mathcal{S}$, and the primary unknowns are the extracellular potential u_e and the transmembrane potential u. Hence, the intracellular potential reads $u_i = u + u_e$. For all $t > 0$, we seek (u, u_e) with $\int_{\mathcal{S}} u_e \, dS = 0$ such that, for all (ϕ, ψ) with $\int_{\mathcal{S}} \psi \, dS = 0$,

$$\begin{cases} A_m \displaystyle\int_{\mathcal{S}} \Big(C_m \frac{\partial u}{\partial t} + I_{\text{ion}}(u) \Big) \phi \, dS + \int_{\mathcal{S}} \Big(\boldsymbol{\sigma}_i \cdot \big(\boldsymbol{\nabla} u + \boldsymbol{\nabla} u_e \big) \Big) \cdot \boldsymbol{\nabla} \phi \, dS \\ \qquad\qquad = A_m \displaystyle\int_{\mathcal{S}} I_{\text{app}} \phi \, dS, \\ \displaystyle\int_{\mathcal{S}} \Big((\boldsymbol{\sigma}_i + \boldsymbol{\sigma}_e) \cdot \boldsymbol{\nabla} u_e \Big) \cdot \boldsymbol{\nabla} \psi \, dS + \int_{\mathcal{S}} \Big(\boldsymbol{\sigma}_i \cdot \boldsymbol{\nabla} u \Big) \cdot \boldsymbol{\nabla} \psi \, dS = 0. \end{cases} \tag{1}$$

Here, the positive constant A_m denotes the ratio of membrane area per unit volume, C_m is the membrane capacitance per unit surface, $I_{\text{ion}}(u)$ a reaction term representing the ionic current across the membrane and also depending on local ionic variables satisfying additional ODEs – in our case we use the ionic model of [8] – and I_{app} a given prescribed stimulus current, when applicable. We define the intra- and extra-cellular diffusion tensors $\boldsymbol{\sigma}_i$ and $\boldsymbol{\sigma}_e$ by

$$\boldsymbol{\sigma}_{i,e} = \sigma_{i,e}^t \boldsymbol{I} + (\sigma_{i,e}^l - \sigma_{i,e}^t) \big[I_0(\theta) \boldsymbol{\tau}_0 \otimes \boldsymbol{\tau}_0 + J_0(\theta) \boldsymbol{\tau}_0^\perp \otimes \boldsymbol{\tau}_0^\perp \big], \tag{2}$$

where $\boldsymbol{I}$ denotes the identity tensor in the tangential plane – also sometimes called the surface metric tensor – $\boldsymbol{\tau}_0$ is a unit vector associated with the local fiber direction on the atria midsurface, and $\boldsymbol{\tau}_0^\perp$ such that $(\boldsymbol{\tau}_0, \boldsymbol{\tau}_0^\perp)$ gives an orthonormal basis of the tangential plane. The functions $I_0(\theta) = \frac{1}{2} + \frac{1}{4\theta} \sin(2\theta)$ and $J_0(\theta) = 1 - I_0(\theta)$ represent the effect of an angular variation 2θ of the fiber direction across the wall. A typical physiological simulation of the model is presented in Fig.1 in a healthy case, with the parameters given in Table 1. For details on the modeling formulation and parameter calibration we refer to [4, 7], and also to [16] where this model was used in the atria for numerical simulations of complete realistic electrocardiograms.

2.2 Data of interest

We assume in this work that the patient-specific depolarization front is measured, as is the case when isochrones are available. From a mathematical standpoint,

Table 1. Conductivity parameters (all in $\mathrm{S.cm}^{-1}$) and maximal conductance g_{Na} in the different atrial areas (all in $\mathrm{nS.pF}^{-1}$) with RT = regular tissue, PM = pectinate muscles, CT = crista terminalis, BB = Bachman's bundle, FO = fossa ovalis

σ_e^t	σ_e^l	σ_i^t	σ_i^l	g_{Na} (RT)	g_{Na} (PM)	g_{Na} (CT)	g_{Na} (BB)	g_{Na} (FO)
$9.0\,10^{-4}$	$2.5\,10^{-3}$	$2.5\,10^{-4}$	$2.5\,10^{-3}$	7.8	11.7	31.2	46.8	3.9

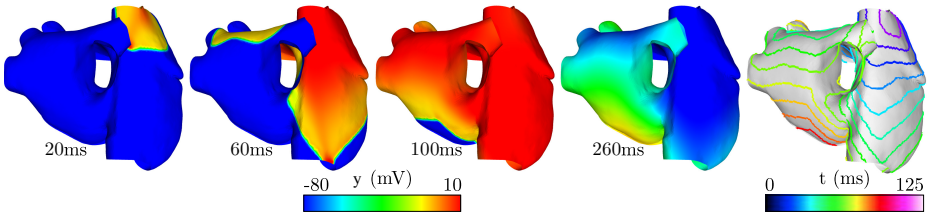

Fig. 1. Atrial electrical depolarization and corresponding synthetic front data

the measurement procedure can be modeled by considering that, for a particular solution of (1) denoted by $(\breve{u}, \breve{u}_e)$ and associated with patient-specific parameters and initial conditions, we have at our disposal the time evolution of the front

$$\Gamma_{\breve{u}}(t) = \{\boldsymbol{x} \in \mathcal{S},\, \breve{u}(\boldsymbol{x}, t) = c_{\mathrm{th}}\}, \tag{3}$$

defining c_{th} as a threshold value characterizing the front, and the already traveled-through region is given by

$$\mathcal{S}_{\breve{u}}^{\mathrm{in}}(t) = \{\boldsymbol{x} \in \mathcal{S},\, \breve{u}(\boldsymbol{x}, t) > c_{\mathrm{th}}\}, \tag{4}$$

up to some measurement noise. These data can be represented as a sequence of images – denoted by $z(t)$ – that essentially take two different values inside and outside the traveled-through region. Our objective is to use the image sequence $z(t)$ to reconstruct the target solution $(\breve{u}, \breve{u}_e)$, in a context where the initial conditions and some physical parameters are uncertain.

3 Estimation methodology

3.1 Sequential estimation principles

We consider a general dynamical system $\dot{y} = A(y, \theta, t)$, where y is the state variable, A the model operator, and θ some parameters of interest. In this abstract setting, we consider a specific target trajectory $\{\breve{y}(t), t > 0\}$ solution of the model with initial condition $\breve{y}(0) = y_\diamond + \breve{\zeta}_y$, where $y_\diamond$ is a known *a priori* whereas $\breve{\zeta}_y$ is unknown, and assuming the same type of decomposition for the parameters $\theta = \theta_\diamond + \breve{\zeta}_\theta$. We further assume that we have at our disposal some indirect measurements of the target trajectory represented by the observation variable $z(t)$. Our estimation problem consists in reconstructing the solution $\{\breve{y}(t), t > 0\}$ and possibly identifying the parameters $\breve{\theta}$ from the data $z(t)$.

As a prerequisite to any estimation strategy, we must be able to define – at each time – a similarity/discrepancy measure $\mathcal{D}(y,z)$ between the data z and the state variable y. When $\mathcal{D}(y,z)$ vanishes, the state is exactly compatible with the data. By contrast, when $\mathcal{D}(y,z)$ is non-zero, the data indicate that $y(t) \neq \breve{y}(t)$.

To achieve our estimation objective, we adopt a so-called *sequential strategy* where we define an *observer* system – also known as *sequential estimator* system – as a new dynamical system of the form

$$\begin{cases} \dot{\hat{y}} = A(\hat{y},\hat{\theta}) + B_y(\mathcal{D},\nabla_y\mathcal{D}), \quad y(0) = y_\diamond, \\ \dot{\hat{\theta}} = B_\theta(\mathcal{D},\nabla_y\mathcal{D}), \quad \hat{\theta}(0) = \theta_\diamond. \end{cases} \tag{5}$$

Here, $B = \left(\begin{smallmatrix} B_y \\ B_\theta \end{smallmatrix}\right)$ is a feedback operator designed with the objective that $(\hat{y},\hat{\theta})$ converge in time to $(\breve{y},\breve{\theta})$, using only the discrepancy measure available at each time. When assuming that $\breve{\zeta}_\theta = 0$, namely, that the model parameters are perfectly known, we choose $B_\theta = 0$, and we then focus on the *state sequential estimator*, also called *state observer*. However, when the parameters must also be identified, the dynamical system (5) defines a *joint state-parameter observer*.

3.2 State observer using shape derivatives

In this paper, we focus on the design of a state observer using the front data. Our objective is to extend the state observer introduced in [6], where a more extensive development of the general methodology is provided, including an additional parameter estimation component. Here, our extended observer will also be compatible with the same parameter estimation strategy.

In [6], the state observer consists in finding for all $t > 0$ the solution $(\hat{u},\hat{u}_e)$ with $\int_{\mathcal{S}} \hat{u}_e \, dS = 0$ such that for all (ϕ,ψ) with $\int_{\mathcal{S}} \psi \, dS = 0$ we have

$$\begin{cases} A_m \displaystyle\int_{\mathcal{S}} \Big(C_m \frac{\partial \hat{u}}{\partial t} + I_{\text{ion}}(\hat{u}) \Big) \phi \, dS + \int_{\mathcal{S}} \Big(\boldsymbol{\sigma}_i \cdot \big(\boldsymbol{\nabla} \hat{u} + \boldsymbol{\nabla} \hat{u}_e \big) \Big) \cdot \boldsymbol{\nabla} \phi \, dS \\ = A_m \displaystyle\int_{\mathcal{S}} I_{\text{app}} \phi \, dS - \lambda \int_{\Gamma_{\hat{u}}} \frac{1}{|\boldsymbol{\nabla} \hat{u}|} \Big(\big(z - C_1(\mathcal{S}_{\hat{u}}^{\text{in}}) \big)^2 - \big(z - C_2(\mathcal{S}_{\hat{u}}^{\text{in}}) \big)^2 \Big) \, \phi \, d\Gamma, \\ \displaystyle\int_{\mathcal{S}} \Big((\boldsymbol{\sigma}_i + \boldsymbol{\sigma}_e) \cdot \boldsymbol{\nabla} \hat{u}_e \Big) \cdot \boldsymbol{\nabla} \psi \, dS + \int_{\mathcal{S}} \Big(\boldsymbol{\sigma}_i \cdot \boldsymbol{\nabla} \hat{u} \Big) \cdot \boldsymbol{\nabla} \psi \, dS = 0. \end{cases} \tag{6}$$

Here, we have

$$\Gamma_{\hat{u}}(t) = \{ \boldsymbol{x} \in \mathcal{S},\, \hat{u}(\boldsymbol{x},t) = c_{\text{th}} \} \text{ and } \mathcal{S}_{\hat{u}}^{\text{in}}(t) = \{ \boldsymbol{x} \in \mathcal{S},\, \hat{u}(\boldsymbol{x},t) > c_{\text{th}} \},$$

which is similar to (3) and (4), but computed with the observer solution $\hat{u}$, $\lambda > 0$ is a constant weighing the confidence in the data, and

$$C_1(\mathcal{S}_{\hat{u}}^{\text{in}}) = \frac{\int_{\mathcal{S}_{\hat{u}}^{\text{in}}} z \, dS}{\int_{\mathcal{S}_{\hat{u}}^{\text{in}}} dS}, \quad C_2(\mathcal{S}_{\hat{u}}^{\text{in}}) = \frac{\int_{\mathcal{S} \setminus \overline{\mathcal{S}_{\hat{u}}^{\text{in}}}} z \, dS}{\int_{\mathcal{S} \setminus \overline{\mathcal{S}_{\hat{u}}^{\text{in}}}} dS}. \tag{7}$$

As discussed in [6] the observer design originates from an analogy with the dynamical behavior of contours tracking an object in a "Mumford-Shah"-based segmentation. Indeed, introducing the data-fitting term of the functional in [3]

$$\mathcal{J}_u = \int_{\mathcal{S}_u^{\text{in}}} \big(z - C_1(\mathcal{S}_u^{\text{in}})\big)^2 \, dS + \int_{\mathcal{S}\setminus\overline{\mathcal{S}_u^{\text{in}}}} \big(z - C_2(\mathcal{S}_u^{\text{in}})\big)^2 \, dS,$$

we can show that the observer data correction term in (6), with respect to the original model (1), corresponds to the *shape derivative* of $\mathcal{J}_u$ given by

$$\boldsymbol{\nabla}_{\text{sh}}\mathcal{J}_u = \frac{\delta_{\Gamma_u}}{|\boldsymbol{\nabla} u|}\Big(\big(z - C_1(\mathcal{S}_u^{\text{in}})\big)^2 - \big(z - C_2(\mathcal{S}_u^{\text{in}})\big)^2\Big),$$

where δ_{Γ_u} is the single-layer distribution associated with the boundary Γ_u, namely, the distribution such that $\int_{\mathcal{S}} \delta_{\Gamma_u}\, \psi \, dS = \int_{\Gamma_u} \psi \, d\Gamma$, for all ψ.

In [6], a mathematical justification was given for the convergence of the observer, at least for "reasonably small" errors. Moreover, numerical tests have demonstrated the effectiveness of this approach, in particular when the target trajectory corresponds to a simple depolarization wave. However, this observer is limited in the sense that it can only correct the front $\Gamma_{\hat{u}}$ that is already present in the simulation. This means that, if we do not have a propagation front to be associated with the data, we are not able to compute any observer correction. Our goal here is to circumvent this limitation, in order to track complex types of propagation patterns such as fibrillations.

3.3 A new state observer based on the topological gradient

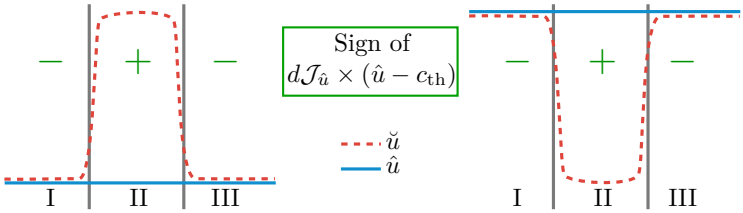

Fig. 2. 1D case example: two opposite topological differences between the observer solution and the data

In order to improve the observer formulation, we intend to follow a strategy of increasing importance in shape optimization [1] or "level-set"-based image segmentation [10, 11]. The central idea is to complement the required shape derivatives, used to modify the shape contours, by a topological derivative that represents the sensitivity of $\mathcal{J}_u$ when removing a small part of the domain. Following [1], we formally define the topological derivative of our functional by

$$d\mathcal{J}_u(\mathcal{S}_u^{\text{in}})(\boldsymbol{x}) = \lim_{\boldsymbol{x}\to 0} \frac{\mathcal{J}_u(\mathcal{S}_u^{\text{in}} \setminus B_{\rho,\boldsymbol{x}}) - \mathcal{J}_u(\mathcal{S}_u^{\text{in}})}{|\mathcal{S}_u^{\text{in}} \cap B_{\rho,\boldsymbol{x}}|}, \quad \forall \boldsymbol{x} \in \mathcal{S}_u^{\text{in}},$$

$B_{\rho,\boldsymbol{x}}$ denoting a ball of radius ρ and center $\boldsymbol{x}$. This gives in our case as in [11]

$$d\mathcal{J}_u(\mathcal{S}_u^{\text{in}})(\boldsymbol{x}) = (z(\boldsymbol{x}) - C_1(\mathcal{S}_u^{\text{in}}))^2 - (z(\boldsymbol{x}) - C_2(\mathcal{S}_u^{\text{in}}))^2. \tag{8}$$

Then, we incorporate this topological derivative in our observer as a new reaction term, when we detect a topological difference between the target solution and the observer solution. In this respect, we follow a simple reasoning inspired from [10] and summarized by the 1D examples of Fig.2, where we show two opposite situations of topological differences. We see that in both cases we want to act only on region II, namely, the region where $d\mathcal{J}_u \times (u - c_{\text{th}})$ is positive. We infer that we should consider a *topological gradient* term of the form

$$\boldsymbol{\nabla}_{\text{top}}\mathcal{J}_u = \Big(1 + \text{sign}\Big(d\mathcal{J}_u \times (u - c_{\text{th}})\Big)\Big) d\mathcal{J}_u,$$

where the first term selects the region where we want to act

$$\Big(1 + \text{sign}\Big(d\mathcal{J}_u \times (u - c_{\text{th}})\Big)\Big) = \begin{cases} 0 & \text{if } \boldsymbol{x} \in I \cup III \\ 2 & \text{if } \boldsymbol{x} \in II \end{cases} \tag{9}$$

while the topological derivative $d\mathcal{J}_u$ provides the direction (creation or destruction, see Fig.2 left and right, respectively).

When incorporating this term in the previous state observer, our new state observer is defined by: find $(\hat{u}, \hat{u}_e)$ with $\int_{\mathcal{S}} \hat{u}_e \, dS = 0$, such that for all $t > 0$,

$$\begin{cases} A_m \displaystyle\int_{\mathcal{S}} \Big(C_m \frac{\partial \hat{u}}{\partial t} + I_{\text{ion}}(\hat{u})\Big)\phi \, dS + \int_{\mathcal{S}} \Big(\boldsymbol{\sigma}_i \cdot \big(\boldsymbol{\nabla}\hat{u} + \boldsymbol{\nabla}\hat{u}_e\big)\Big) \cdot \boldsymbol{\nabla}\phi \, dS \\ \qquad\qquad = -\displaystyle\int_{\mathcal{S}} \Big(\lambda \boldsymbol{\nabla}_{\text{sh}}\mathcal{J}_{\hat{u}} + \mu \boldsymbol{\nabla}_{\text{top}}\mathcal{J}_{\hat{u}}\Big)\phi \, dS + A_m \displaystyle\int_{\mathcal{S}} I_{\text{app}}\phi \, dS, \\ \displaystyle\int_{\mathcal{S}} \Big((\boldsymbol{\sigma}_i + \boldsymbol{\sigma}_e) \cdot \boldsymbol{\nabla}\hat{u}_e\Big) \cdot \boldsymbol{\nabla}\psi \, dS + \int_{\mathcal{S}} \Big(\boldsymbol{\sigma}_i \cdot \boldsymbol{\nabla} u\Big) \cdot \boldsymbol{\nabla}\psi \, dS = 0, \end{cases} \tag{10}$$

with λ, μ two strictly positive constants.

4 Results

4.1 1D test case

As a first illustration and assessment, we consider a monodomain version of (1) coupled with a simple Mitchell-Schaeffer ionic model, in a 1D domain, see [6]. In Fig.3 we compare the performances of the observer of [6] with those of our new observer, in a case where the initial condition is shifted in one area (to the left) and entirely misses another depolarized area (right). Moreover, we show in the bottom row of Fig.3 the results obtained when adding a Gaussian noise of 30% in the data – namely, directly added to $z(t)$, here.

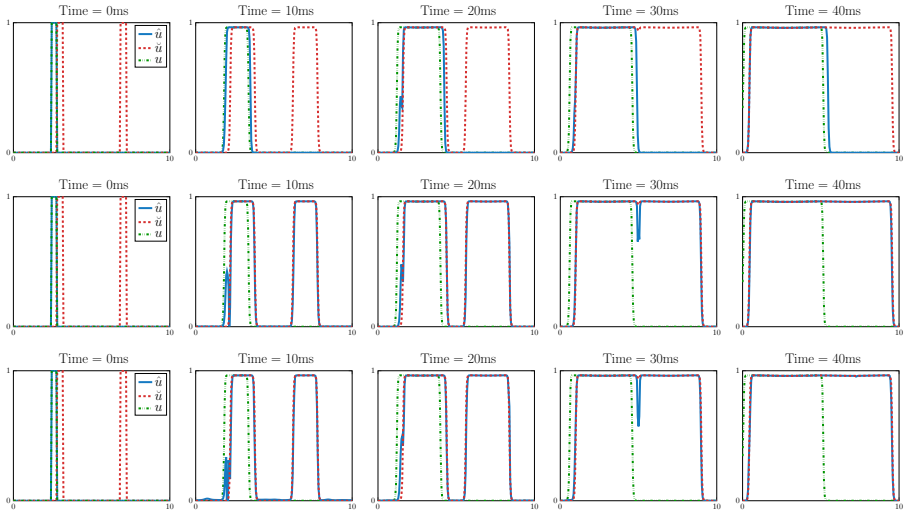

Fig. 3. Comparison of 1D observer based on the shape gradient only (top), and with topological gradient (middle); topological gradient observer with a Gaussian noise of 30% in the data (bottom)

4.2 Atrial fibrillation example

We proceed to consider a more realistic configuration where we purport to track an atrial fibrillation starting from a physiologically "healthy" initial condition. In order to synthetically generate the atrial fibrillation, we use a standard S1-S2 protocol [5]. The location of the stimulation S2 is near the left pulmonary inferior vein. Indeed, the pulmonary veins are known to be prone to frequent re-entries. The S1 stimulus corresponds to a standard sinus stimulation (natural pacemaker of the heart) at t = 0 and t = 700 ms, corresponding to the cardiac cycle period considered here. The S2 stimulus is triggered at t = 290 ms. The results of the simulation of the target atrial fibrillation are displayed in Fig.4 (left column). The figure shows successive time steps between t = 300 ms (note that before the S2 stimulus the simulation is the same as in the healthy case) and t = 820 ms, and compares the reference solution with the results obtained with our observer, and with a direct model simulation undergoing S1 stimulation only like the observer. We also show in Fig.5 the results obtained when considering noisy data, in this case Gaussian noise added to the depolarization times, see the corresponding isochrones in the figure.

5 Discussion

Concerning the 1D simulations, we see in Fig.3 that the original observer of [6] nicely tracks the first depolarized area, but is completely unable to adapt to the other area, hence also when the two areas merge. By contrast, our new observer

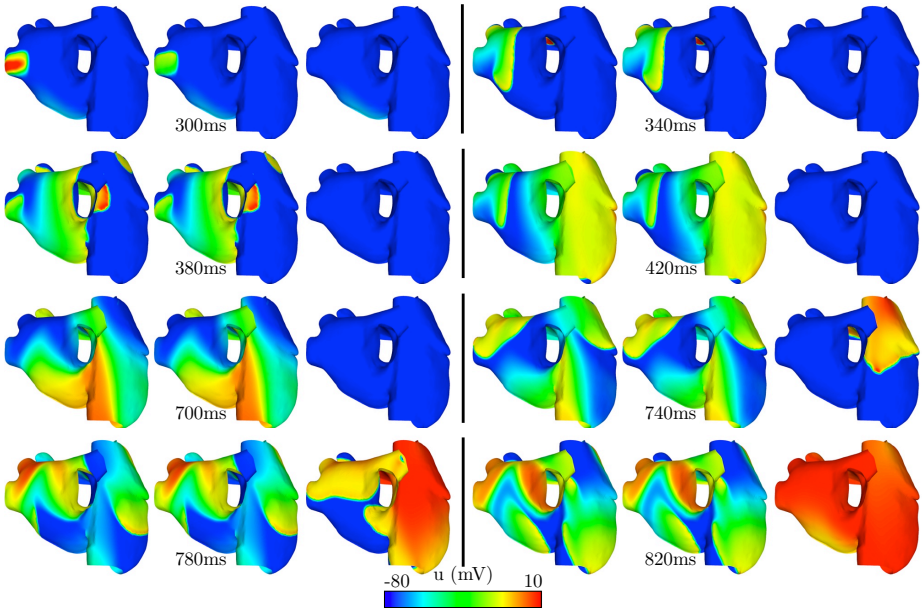

Fig. 4. Atrial fibrillation: target solution (left), observer solution (middle) and direct simulation without data (right)

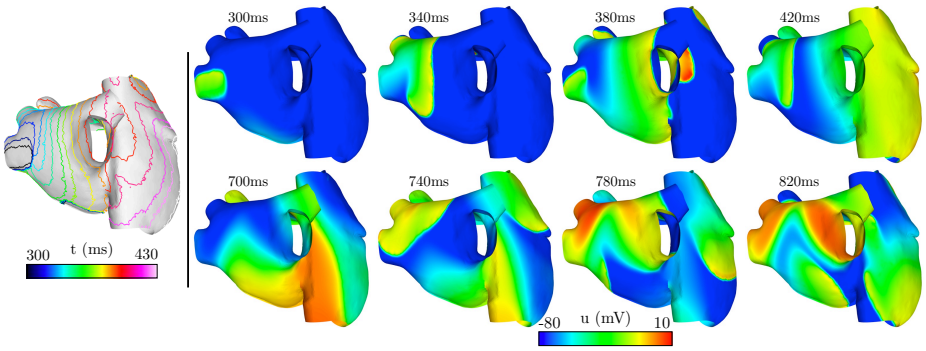

Fig. 5. Atrial fibrillation: synthetic front data with noise (left, note that only the first times of passage after the onset of fibrillation are displayed, for the sake of clarity), and corresponding observer solutions (right)

very effectively retrieves the complete solution. Moreover, the trial with added Gaussian noise shows that our method is very robust to a rather high level of noise, as will be the case with real data.

As regards the atrial fibrillation example, we see in Fig.4 that the observer very quickly and accurately captures the complex nature of the fibrillation solution, even though the initial condition of the system was devised to generate a healthy depolarization. Here again, the sensitivity to noisy data has been further assessed and confirms the robustness of our approach. Therefore, we can envision in future works to reconstruct the state solution from real isochrone data, thereby complementing classical ECGI approaches, as a second step after the ECGI wavefront inverse problem formulation reviewed e.g. in [5, Section 6.5].

Further perspectives include extending the present observer to perform state-parameter estimation, which is straightforward using the strategy originally proposed in [13], see also [6]. Of course, our method is also applicable in principle to 3D electrophysiology models – as would be adequate for ventricular electrophysiology – albeit directly so only with isochrone *surfaces*, which is not generally how actual data are available – more often in the form of lines within outer surfaces (epi- and/or endocardium). Therefore some degree of adaptation is needed to incorporate such clinical data in a 3D observer system. Of course, ultimately some assessments are required in real clinical cases with actual data.

6 Concluding remarks

We have proposed a new observer for performing estimation in an electrophysiology model with data in the form of level sets of the electrical potential. Our method builds up on a previously-proposed observer based on shape derivatives, and incorporates a new term based on the topological gradient concept, in order to allow the tracking of solutions of complex topological structures, as e.g. in fibrillation cases. Our assessments have demonstrated the effectiveness of this approach, including in a realistic case of atrial fibrillation. We also emphasize that our approach is conceptually general, hence it can be applied to other models of propagative reaction-diffusion type – as e.g. for wild-fire propagation – in a very straightforward manner.

Acknowledgment: The research leading to these results has received partial funding from the European Union's Seventh Framework Programme for research, technological development and demonstration, under grant agreement #611823 (VP2HF Project).

References

1. M. Burger, B. Hackl, and W. Ring. Incorporating topological derivatives into level set methods. *Journal of Computational Physics*, 194(1):344–362, 2004.
2. R. Chabiniok, P. Moireau, A. Lesault, P.-F.and Rahmouni, J.-F. Deux, and D. Chapelle. Estimation of tissue contractility from cardiac cine-MRI using

a biomechanical heart model. *Biomechanics and Modeling in Mechanobiology*, 11(5):609–30, 2012.

3. T.F. Chan and L.A. Vese. Active contours without edges. *IEEE Transactions on Image Processing*, 10(2):266–277, 1991.
4. D. Chapelle, A. Collin, and J.-F. Gerbeau. A surface-based electrophysiology model relying on asymptotic analysis and motivated by cardiac atria modeling. *M3AS*, 23(14):2749–2776, 2013.
5. P. Colli Franzone, L.F. Pavarino, and S. Scacchi. *Mathematical Cardiac Electrophysiology*, volume XIV of *MS&A*. Springer, 2014.
6. A. Collin, D. Chapelle, and P. Moireau. A Luenberger observer for reaction-diffusion models with front position data. Preprint available in HAL electronic archive, 2014.
7. A. Collin, J.-F. Gerbeau, M. Hocini, M. Haïssaguerre, and D. Chapelle. Surface-based electrophysiology modeling and assessment of physiological simulations in atria. *FIMH 2013*, 7945:352–359, 2013.
8. M. Courtemanche, R.J. Ramirez, and S. Nattel. Ionic mechanisms underlying human atrial action potential properties: insights from a mathematical model. *American Journal of Physiology*, 275:H301–H321, 1998.
9. O. Doessel, M.W. Krueger, F.M. Weber, C. Schilling, W.H.W. Schulze, and G. Seemann. A framework for personalization of computational models of the human atria. In *EMBC, 2011*, pages 4324–28, 2011.
10. L. He, C.Y. Kao, and S. Osher. Incorporating topological derivatives into shape derivatives based level set methods. *Journal of Computational Physics*, 225(1):891–909, 2007.
11. M. Hintermüller and A. Laurain. Multiphase image segmentation and modulation recovery based on shape and topological sensitivity. *Journal of Mathematical Imaging and Vision*, 35(1):1–22, 2009.
12. E. Konukoglu, O. Clatz, B. H. Menze, B. Stieltjes, M.-A. Weber, E. Mandonnet, H. Delingette, and N. Ayache. Image guided personalization of reaction-diffusion type tumor growth models using modified anisotropic eikonal equations. *Medical Imaging, IEEE Transactions*, 29(1):77–95, 2010.
13. P. Moireau and D. Chapelle. Reduced-order Unscented Kalman Filtering with application to parameter identification in large-dimensional systems. *ESAIM: Control, Optimisation and Calculus of Variations*, 17(2):380–405, 2011.
14. V. Moreau-Villeger, H. Delingette, M. Sermesant, H. Ashikaga, E. McVeigh, and N. Ayache. Building maps of local apparent conductivity of the epicardium with a 2-D electrophysiological model of the heart. *IEEE Trans. Biomed. Eng.*, 53(8):1457–1466, 2006.
15. C. Ramanathan, R.J. Ghanem, P. Jia, K. Ryu, and Y. Rudy. Noninvasive electrocardiographic imaging for cardiac electrophysiology and arrhythmia. *Nature Medicine*, 10:422–428, 2004.
16. E. Schenone, A. Collin, and J.-F. Gerbeau. Numerical simulations of full electrocardiogram cycle. *Accepted for publication in IJNMBE*, 2015.
17. N. Smith, A. de Vecchi, M. McCormick, D. Nordsletten, O. Camara, A.F. Frangi, H. Delingette, M. Sermesant, J. Relan, N. Ayache, M.W. Krueger, W.H.W. Schulze, R. Hose, I. Valverde, P. Beerbaum, C. Staicu, M. Siebes, J. Spaan, P. Hunter, J. Weese, H. Lehmann, D. Chapelle, and R. Rezavi. euHeart: personalized and integrated cardiac care using patient-specific cardiovascular modelling. *Interface Focus*, 1(3):349–364, 2011.